Genotype-phenotype correlation of tracheal cartilaginous sleeves and *Fgfr2* mutations in mice

Austin S Lam, MD[1,2,3], **C Carrie Liu, MD MPH**[1,2,*], **Gail H Deutsch, MD**[4,5], **Joshua Rivera, BS**[6,**], **Jonathan A Perkins, DO**[1,2,8], **Greg Holmes, PhD**[6], **Ethylin Wang Jabs, MD**[6], **Michael L Cunningham, MD PhD**[3,7,8], **John P Dahl, MD PhD MBA**[1,2,8]

[1] =Department of Otolaryngology – Head & Neck Surgery, University of Washington School of Medicine, Seattle, WA

[2] =Division of Pediatric Otolaryngology – Head & Neck Surgery, Seattle Children's Hospital, Seattle, WA

[3] =Seattle Children's Research Institute, Center for Developmental Biology and Regenerative Medicine, Seattle, WA

[4] =Department of Pathology, University of Washington School of Medicine, Seattle, WA

[5] =Department of Pathology, Seattle Children's Hospital, Seattle, WA

[6] =Department of Genetics and Genomic Sciences, Icahn School of Medicine at Mount Sinai, New York City, NY

[7] =Department of Pediatrics, University of Washington School of Medicine, Seattle, WA

[8] =Craniofacial Center, Seattle Children's Hospital, Seattle, WA

Abstract

Objectives: To characterize tracheal cartilage morphology in mouse models of *Fgfr2*-related craniosynostosis syndromes. To establish relationships between specific *Fgfr2* mutations and tracheal cartilaginous sleeve (TCS) phenotypes in these mouse models.

Methods: Postnatal day-0 knock-in mouse lines with disease specific genetic variations in the *Fgfr2* gene (*Fgfr2*[C342Y/C342Y], *Fgfr2*[C342Y/+], *Fgfr2*[+/Y394C], *Fgfr2*[+/S252W] and *Fgfr2*[+/P253R]) as well as line-specific controls were utilized. Tracheal cartilage morphology as measured by gross analyses, microcomputed-tomography, and histopathology were compared using Chi-squared and single-factor analysis of variance statistical tests.

Results: A greater proportion of rings per trachea were abnormal in *Fgfr2*[C342Y/+] tracheas (63%) than *Fgfr2*[+/S252W] (17%), *Fgfr2*[+/P253R] (17%), *Fgfr2*[+/Y394C] (12%) and controls (10%) ($p < .001$ for each vs *Fgfr2*[C342Y/+]). TCS segments were found only in *Fgfr2*[C342Y/C342Y] (100%) and *Fgfr2*[C342Y/+] (72%) tracheas. Cricoid and 1st tracheal ring fusion was noted in all

Corresponding Author: John P Dahl, MD PhD MBA, (206) 987-2105, John.Dahl@seattlechildrens.org.
* =Current address: Divisions of Otolaryngology – Head and Neck Surgery, and Pediatric Surgery, Department of Surgery, University of Calgary, Calgary, AB
** =Current address: Center for Personalized Cancer Therapy, University of Massachusetts, Boston, MA

$Fgfr2^{C342Y/C342Y}$ and 94% of $Fgfr2^{C342Y/+}$ samples. The $Fgfr2^{C342Y/C342Y}$ and $Fgfr2^{C342Y/+}$ groups were found to have greater areas and volumes of cartilage than other lines on gross analysis and microcomputed-tomography. Histologic analyses confirmed TCS among the $Fgfr2^{C342Y/C342Y}$ and $Fgfr2^{C342Y/+}$ groups, without appreciable differences in cartilage morphology, cell size or density; no histologic differences were observed among other $Fgfr2$ lines compared to controls.

Conclusion: This study found TCS phenotypes only in the $Fgfr2^{C342Y}$ mouse lines. These lines also had increased tracheal cartilage compared to other mutant lines and controls. These data support further study of the $Fgfr2$ mouse lines and the investigation of other $Fgfr2$ variants to better understand their role in tracheal development and TCS formation.

Keywords

FGFR2; tracheal cartilaginous sleeve; tracheal anomalies; craniosynostosis; Crouzon syndrome; Apert syndrome; Beare-Stevenson syndrome

Introduction:

Tracheal cartilaginous sleeve (TCS) is a life-threatening airway malformation often found in patients with syndromic craniosynostosis.[1] The condition results from the vertical fusion of tracheal rings – forming a solid C-shaped "sleeve" of cartilage along the anterior and lateral trachea.[2] Abnormal airway architecture in those with TCS is thought to alter airway dynamics and airway clearance, and may not allow adequate airway growth to support the respiratory requirements of a developing child.[3] A 90% mortality rate has been reported by 2 years of age without tracheotomy.[4]

With the exception of rare reports, TCS is associated only with craniosynostosis syndromes caused by mutations in fibroblast growth factor receptor 2 (FGFR2), such as Apert, Beare-Stevenson, Crouzon, and Pfeiffer syndromes.[3,5] The FGFRs are a family of four receptor tyrosine kinases, each composed of a split intracellular-kinase domain, single transmembrane domain, and ligand-binding extracellular domain. The extracellular domain contains three immunoglobulin (Ig)-like domains, with ligand binding occurring at the second and third Ig-like domains. The receptors dimerize when complexed with fibroblast growth factors (FGFs) or other receptor-specific signaling molecules. This dimerization leads to the activation of downstream signaling cascades involved in a wide array of cellular responses including regulation of cell proliferation, differentiation and migration.[6–8] Gain-of-function mutations upregulate these processes and are associated with the aforementioned craniosynostoses syndromes.[7]

Protein variants FGFR2^{C342Y} (p.Cys342Tyr) and FGFR2^{Y375C} (p.Tyr375Cys) are associated with Crouzon and Beare-Stevenson syndromes, respectively, and result in ligand-_independent_ FGFR2 activation.[8–12] Meanwhile, variants FGFR2^{S252W} (p.Ser252Trp) and FGFR2^{P253R} (p.Pro253Arg) account for 98% of mutations seen in human Apert syndrome. Both occur at the linker-region between Ig-like loops II and III and enhance receptor binding affinity, resulting in ligand-_dependent_ activation of FGFR2.[7,12,13]

While TCS has been described in patients with several different FGFR2 mutations, a clear genotype-phenotype relationship has not been established. Such a relationship is of clinical importance as TCS is notoriously difficult to diagnose and early treatment is critical.[3] In this study, we systematically characterized tracheal cartilage morphology using knock-in mouse models of ligand-*independent* (Crouzon/$Fgfr2^{C342Y}$, Beare-Stevenson/$Fgfr2^{Y394C}$) and ligand-*dependent* (Apert/$Fgfr2^{S252W}$ and $Fgfr2^{P253R}$) activation to establish genotype-phenotype correlations.

We hypothesized that genotype-phenotype correlation would be demonstrated and that mice with ligand-*independent* activating *Fgfr2* mutations would demonstrate TCS that are more severe and occur at greater frequency than those with ligand-*dependent* *Fgfr2* mutations.

Materials and Methods:

Animal models and preparation:

Generation of mouse models are described elsewhere.[14–17] $Fgfr2^{C342Y/(C342Y/+)}$ mice were maintained on a CD1 outbred background whereas $Fgfr2^{+/Y394C}$, $Fgfr2^{+/S252W}$ and $Fgfr2^{+/P253R}$ mice were maintained on C57BL/6J inbred backgrounds. Line-specific controls were utilized for analyses ($Fgfr2^{+/+}$). Mouse lines were maintained at the Icahn School of Medicine for ongoing experiments. Previous studies have demonstrated high neonatal lethality rates for mice with $Fgfr2^{C342Y/C342Y}$, $Fgfr2^{+/S252W}$ and $Fgfr2^{+/P253R}$ genotypes.[15–17] Thus, postnatal day-0 (P0) mice were euthanized per local Institutional Animal Care and Use Committee (IACUC) protocols. Mouse thoraces were harvested and fixed in 4% paraformaldehyde. Tracheas were dissected and removed *en bloc* with thyroid cartilages and mainstem bronchi. Genotype was determined using line specific PCR assays.[14–17] Animal protocols were approved by the Icahn School of Medicine Institutional Animal Care and Use Committee.

Tracheal morphology evaluation:

Tracheas were fixed in 95% ethanol. Alcian blue staining was carried out according to standard protocols.[18]

Alcian blue-stained tracheas were examined under stereomicroscopy (Nikon Instruments Inc., Melville, NY) and rings individually classified according to a modified version of the classification system described by Permakumar et al.[19] "Normal" ring types were defined as those present on at least 20% of control specimens. "Abnormal" ring types were present on fewer than 20% of control tracheas and those classified as "Other". Two sleeve-type ring segments were defined: "Complete cartilaginous sleeve" and "Partially sleeved rings." A tracheal segment was defined as 1/3rd tracheal length – superior, middle, inferior. Analysis was performed for 86 specimens (n = 5 $Fgfr2^{C342Y/C342Y/+}$; 32 $Fgfr2^{C342Y/+}$; 5 $Fgfr2^{+/Y394C}$; 6 $Fgfr2^{+/S252W}$; 5 $Fgfr2^{+/P253R}$; 33 $Fgfr2^{+/+}$). The ring type classification system is detailed in Figure 1.

The presence or absence of fusion of the cricoid and 1st tracheal rings were noted.

Cartilage dimensions assessment:

Images of 80 alcian blue whole-mount stained tracheas ($n = 5$ $Fgfr2^{C342Y/C342Y/+}$; 30 $Fgfr2^{C342Y/+}$; 5 $Fgfr2^{+/Y394C}$; 5 $Fgfr2^{+/S252W}$; 5 $Fgfr2^{+/P253R}$; 30 $Fgfr2^{+/+}$) were obtained in an anterior-to-posterior orientation. Using these images, photographic area containing stained cartilage was manually highlighted and extracted using Adobe Photoshop CC 2017.0.0 (Adobe Inc., San Jose, CA) and imported into ImageJ software 1.52a (National Institutes of Health) where cartilage area was calculated.[20] Only the cartilage present between the superior border of the cricoid cartilage and the carina was included. Thus, the amount of cartilage visible on the 2-dimensional images, was quantified as cartilage area.

Methods for additional cartilage dimensions are provided in Supplemental Methods.

Microcomputed-tomography assessment:

After serial alcohol dehydration tracheas were stained in 1% phosphotungstic acid for 7 days and then washed with tap water.[21] Microcomputed-tomography (μCT) was performed using a SkyScan-1076 microtomography system (Bruker Corporation, Billerica, MA). μCT settings are provided in Supplemental Methods. Images were reconstructed with NRecon v1.7.0.4. software (Bruker Corporation, Billerica, MA) for segmentation and data acquisition with 3D Slicer v4.11.0 (www.slicer.org).[22]

Volumetric models of tracheal cartilage and airway lumens were obtained by manual segmentation. Cartilage and airway volumes between the superior border of the cricoid cartilage and the inferior-most point of the common tracheal airway were calculated using the Segment Statistics module. Cross-sectional areas along the entire airway lumen were computed and the mean and minimum cross-sectional areas, as well as the cross-sectional area at the cricoid, were recorded. Tracheal cartilage volumes were obtained for 35 samples ($n = 4$ $Fgfr2^{C342Y/C342Y/+}$; 5 $Fgfr2^{C342Y/+}$; 3 $Fgfr2^{+/Y394C}$; 3 $Fgfr2^{+/S252W}$; 4 $Fgfr2^{+/P253R}$; 16 $Fgfr2^{+/+}$) and airway volumes for 33 ($n = 4$ $Fgfr2^{C342Y/C342Y/+}$; 4 $Fgfr2^{C342Y/+}$; 2 $Fgfr2^{+/Y394C}$; 3 $Fgfr2^{+/S252W}$; 4 $Fgfr2^{+/P253R}$; 16 $Fgfr2^{+/+}$).

Histopathologic evaluation:

Fixed tracheas were paraffin-embedded, sectioned at 5 microns and stained with hematoxylin and eosin and Movat pentachrome. Images were captured with a digital camera mounted on a Nikon Eclipse 80i microscope and analyzed using NIS-Elements Advanced Research Software v4.13 (Nikon Instruments Inc., Melville, NY). The number of chondrocytes per area of hyaline cartilage was assessed on 5 random images taken at 40x for 2 samples per group. The number of chondrocytes is expressed as a fraction of the total cartilage area. All sections were reviewed by a board-certified pathologist with expertise in airway histopathology (GHD).

Statistical analysis:

Statistical analysis was performed using the Real Statistics Resource Pack Software v6.8.1.[23] Chi-squared statistic with *post hoc* Fisher Exact Test was utilized to compare groups for categorical variables. For continuous variables, two-tailed T-Test assuming equal variances was used for comparisons involving two groups, and single-factor analysis of

variance (ANOVA) with *post hoc* Tukey HSD was used for comparisons with greater than two groups. An alpha level of 0.05 was used for all statistical procedures. Frequencies are reported for categorical variables whereas means ± standard deviations are reported for continuous variables.

Line-specific control groups were pooled for analyses between *Fgfr2* variant groups.

Results:

Tracheal morphology evaluation:

Representative whole-mount images are provided in Figure 2A–F. The mean proportions of abnormal rings per trachea for the $Fgfr2^{C342Y/C342Y}$ (100±0%) and $Fgfr2^{C342Y/+}$ (63±27%) groups were significantly greater than all other groups, which were similar to controls (10±8%) ($p < .001$ $Fgfr2^{C342Y/C342Y}$ and $Fgfr2^{C342Y/+}$ vs each other group) ($F_{(5, 80)} =$ 43.49, $p < .001$) (Table 1, Figure 2G).

Sleeve-type segments were present only in $Fgfr2^{C342Y/C342Y}$ (100%) and $Fgfr2^{C342Y/+}$ (72%) tracheas (X^2 (5, $N = 86$) = 56.54, $p < .001$). The mean proportion of sleeve-type segments per trachea was greater in the $Fgfr2^{C342Y/C342Y}$ group (100±0%) than all other groups ($p < .001$ for $Fgfr2^{C342Y/C342Y}$ vs each group) ($F_{(5, 80)} = 35.36$, $p < .001$). Greater mean proportion of sleeve-type segments per trachea was also noted among the $Fgfr2^{C342Y/+}$ group (23±27%) as compared to the $Fgfr2^{+/S252W}$ (0±0%, $p = 0.04$) and $Fgfr2^{+/+}$ (0±0%, $p < .001$) groups. It was also observed that sleeve-type segments tended to be present on the superior trachea, whereas the inferior trachea tended to have more normal appearing rings. No sleeve-type segments were present in any other group (Figure 2A–F).

Cricoid and 1st tracheal ring fusion was noted in all $Fgfr2^{C342Y/C342Y}$ and 94% of $Fgfr2^{C342Y/+}$ tracheas. These frequencies were significantly greater than in all other groups, in which no cricoid and 1st tracheal ring fusion was found in any specimen ($p < .001$ for $Fgfr2^{C342Y/C342Y}$ and $Fgfr2^{C342Y/+}$ vs each other group) (X^2 (5, $N = 86$) = 78.23, $p < .001$).

Cartilage dimensions assessment:

Significant between group differences in whole-mount mean cartilage area among mutant groups were found ($F_{(5, 74)} = 38.03$, $p < .001$). Cartilage area values for each group are provided in Table 2. The mean cartilage area for the $Fgfr2^{C342Y/C342Y}$ group was significantly greater than all other groups ($p < .001$ for all comparisons). The $Fgfr2^{C342Y/+}$ group was the greatest among the heterozygous groups, significantly greater than the $Fgfr2^{+/Y394C}$, $Fgfr2^{+/S252W}$ and $Fgfr2^{+/+}$ groups ($p < .001$ for each comparison). The mean cartilage area for the $Fgfr2^{+/P253R}$ group was noted to be significantly greater than the $Fgfr2^{+/Y394C}$ ($p = .04$) and $Fgfr2^{+/+}$ ($p = .01$) groups (Figure 2H).

Microcomputed-tomography assessment:

Representative μCT images are provided in Figure 3A–F. Among *Fgfr2* variants, a significant between group difference was identified ($F_{(5, 29)} = 27.10$, $p < .001$). Cartilage volume values for each group are provided in Table 3. Mean cartilage volume was greatest among $Fgfr2^{C342Y/C342Y}$ tracheas, followed by the $Fgfr2^{C342Y/+}$ group. The $Fgfr2^{+/+}$ group

demonstrated the lowest mean cartilage volume, followed by the $Fgfr2^{+/S252W}$ group. Mean cartilage volume for $Fgfr2^{C342Y/C342Y}$ tracheas was significantly greater than all other groups ($p < .001$ for all comparisons) and mean volume among $Fgfr2^{C342Y/+}$ tracheas was significantly greater than $Fgfr2^{+/+}$ tracheas ($p < .001$). There was a trend for greater mean cartilage volume in the $Fgfr2^{C342Y/+}$ group as compared to $Fgfr2^{+/Y394C}$ ($p = 0.1$) and $Fgfr2^{+/S252W}$ ($p = .05$) tracheas but significance was not reached (Figure 3G).

A significant between group difference in mean airway volumes was detected ($F(5, 27) = 3.34$, $p = .02$). Airway volume values for each group are provided in Table 3. Mean airway volume was greatest among $Fgfr2^{C342Y/C342Y}$ tracheas and least in the $Fgfr2^{+/S252W}$ group. Airway volume was similar among $Fgfr2^{C342Y/+}$ and $Fgfr2^{+/Y394C}$ tracheas, whereas the $Fgfr2^{+/P253R}$ group demonstrated volumes similar to the $Fgfr2^{+/+}$ group. The $Fgfr2^{C342Y/C342Y}$ group demonstrated significantly greater mean airway volumes than both the $Fgfr2^{+/S252W}$ and $Fgfr2^{+/+}$ groups ($p = .02$ and $p = .03$, respectively). No other between group differences for airway volume reached statistical significance (Figure 3H).

Histopathologic evaluation:

Representative histopathologic images are provided in Figure 4A–D. Microscopic examination of coronal and transverse tracheal sections confirmed the presence of TCS in the $Fgfr2^{C342Y/C342Y}$ and $Fgfr2^{C342Y/+}$ groups (Figure 4B,D). All other groups appeared similar to the representative images in Figure 4A,C. No other consistent structural abnormalities were seen in hyaline cartilage rings, trachealis muscles or intercartilaginous spaces. There were no distinguishable abnormalities in chondrocyte cytologic appearance, cell size, or presence of binucleated forms among groups, compared to their line-specific controls. Occasional mitotic figures within chondrocytes were seen in all cases (Figure 4C, D). Morphometric assessment of cell density per cartilage area demonstrated no significant between group differences ($F(5, 12) = 1.30$, $p = .3$) (Figure 4E).

Additional data:

Data for comparisons with individual line-specific control groups are provided in Supplemental Tables S1–S4. Additional $Fgfr2$ variant comparison data from evaluations of tracheal morphology, tracheal cartilage dimensions, microcomputed-tomography and histology is presented in Supplemental Table S5.

Discussion:

Given the significant clinical impact of TCS phenotypes, we evaluated tracheal morphology using knock-in mouse models of $Fgfr2$-associated craniosynostosis syndromes. The analysis included mouse models harboring either ligand-*independent* ($Fgfr2^{C342Y}$, $Fgfr2^{Y394C}$) or ligand-*dependent* ($Fgfr2^{S252W}$, $Fgfr2^{P253R}$) activating mutations.[14–17] We hypothesized that a genotype-phenotype correlation for TCS malformations would be demonstrated among the tested mouse lines and found that tracheal abnormalities were more frequent and severe among $Fgfr2^{C342Y}$ lines. We also hypothesized that ligand-*independent* activating $Fgfr2$ mutations would be associated with TCS malformations at greater incidence and severity

than ligand-*dependent* mutations. While this was seen in $Fgfr2^{C342Y}$ tracheas, it was not observed in the other ligand-*independent* group ($Fgfr2^{Y394C}$).

The $Fgfr2^{C342Y/C342Y}$ group was most severely affected, with all tracheas demonstrating exclusively sleeve-type segments. Further, these tracheas exhibited greater amounts of cartilage and tracheal airway volumes. The presence of larger tracheal airways is interesting since tracheal stenosis has been thought possibly associated with TCS.[24,25] It is theorized that the tube-like cartilage in TCS may fail to appropriately increase in size with patient growth, leading to a relatively stenotic airway.[3] Since our study utilized a single experimental time point, we could not assess the impact of airway growth on stenosis. It is also possible that this observation was an artifact of fixation, with reduced dehydration-related contraction possibly associated with greater amounts of cartilage (as in TCS). Airways did appear smaller in the $Fgfr2^{+/S252W}$ group but were otherwise similar among heterozygous mutants and controls. Since tracheal cartilage abnormalities were generally not found in the $Fgfr2^{+/S252W}$ group, this difference in airway size is likely due to smaller body size, as opposed to morphologically abnormal tracheas. While body size was not assessed in our study, other research has shown P0 mice with the $Fgfr2^{S252W}$ mutation to be smaller than controls.[16] Previous studies of P0 $Fgfr2^{+/Y394C}$ and $Fgfr2^{+/P253R}$ mice showed no difference in body size when compared to controls.[14,17]

Of the heterozygous groups, the $Fgfr2^{C342Y/+}$ tracheas were most severely affected. Nearly all samples in this group were noted to have fusion of the cricoid and 1st tracheal ring – a finding not observed in any other heterozygous or control sample. $Fgfr2^{C342Y/+}$ tracheas were also the only heterozygous specimens exhibiting sleeve-type segments, present in 75% of $Fgfr2^{C342Y/+}$ tracheas. This prevalence is substantially greater than that reported in children with the mutation.[3] Frequent use of bronchoscopy as a diagnostic modality in human studies may result in under-diagnosis of TCS, as the subtle and non-specific endoscopic findings make diagnosing TCS extremely difficult.[2,3] Noorily et al., observed TCS in humans that frequently did not involve the entire trachea.[26] Likewise, we describe a large number of tracheas with sleeved segments that do not extend the entire tracheal length. Bronchoscopy in patients with morphologically similar tracheas would be unlikely to yield a TCS diagnosis since visualization of defined tracheal ring structures could lower the surgeon's index of suspicion.

Non-sleeve-type rings were also abnormal at high frequencies in $Fgfr2^{C342Y/+}$ tracheas. In this group, the average proportion of non-sleeve-type abnormal rings per trachea was 40%, whereas other heterozygous groups were similar to controls (10%). The TCS entity has been described as a broad spectrum of cartilaginous abnormalities; samples without overt TCS, but larger burdens of morphologically abnormal rings may represent the more limited disease extent on this spectrum.[26]

To further examine the spectrum of tracheal cartilage abnormalities and compare genotypes, we quantified the amount of tracheal cartilage by calculating the area of stained cartilage on anterior-posterior photographs and by measuring cartilage volume on µCT scans. Of the heterozygous groups, $Fgfr2^{C342Y/+}$ had the greatest amounts of cartilage followed by the $Fgfr2^{+/P253R}$ group; the $Fgfr2^{+/Y394C}$ and $Fgfr2^{+/S252W}$ groups had measurements similar to

controls. Greater amounts of cartilage in $Fgfr2^{+/P253R}$ mice (ligand-*dependent* activation) than in $Fgfr2^{+/Y394C}$ mice (ligand-*independent* activation) was contrary to our hypothesis – that ligand-*independent* mutations would be associated with TCS at greater incidence and severity than ligand-*dependent* mutations. Despite activating the same receptor type, different mutations in *Fgfr2* may cause differential activation of downstream signaling cascades in different tissues.[14] Thus, the $Fgfr2^{P253R}$ mutation may result in signaling upregulation that, to a greater degree, affects pathways involved in tracheal cartilage formation. Interestingly, whereas the Apert-associated variant $FGFR2^{S252W}$ is more commonly associated with TCS in humans, the $Fgfr2^{P253R}$ mutation was associated with greater amounts of tracheal cartilage in our study.[3,27] While this finding may also be explained by differential signaling cascade stimulation, another possible explanation would be greater overall *Fgfr2* activation in the $Fgfr2^{P253R}$ variant. Both the $Fgfr2^{P253R}$ and $Fgfr2^{S252W}$ mutations affect the linker region between the Ig-like II and III domains, and both are associated with reduced ligand dissociation.[9] However, whereas the increased affinity in the $Fgfr2^{S252W}$ variant is *ligand-specific*, the $Fgfr2^{P253R}$ mutation results in an *indiscriminate* increased affinity for FGFs.[7] Indiscriminate *Fgfr2* activation in the $Fgfr2^{P253R}$ group may lead to greater signaling pathway upregulation with subsequently increased abnormal tracheal cartilage development. Genotype-phenotype correlations between *Fgfr2* mutations and cartilage phenotypes also may vary with the location or structure of the cartilage. In a study of midface phenotypes of $Fgfr2^{C342Y/+}$, $Fgfr2^{+/S252W}$ and $Fgfr2^{+/P253R}$ mutants, increased thickness of nasal cartilages were seen in $Fgfr2^{+/S252W}$ and $Fgfr2^{+/P253R}$ variants.[28] A comparison of Meckel's cartilage between these three genotypes again found significantly increased cartilage thickness only in $Fgfr2^{+/S252W}$ and $Fgfr2^{+/P253R}$ mutants.[29]

Genetic and phenotypic variability exists within craniosynostosis syndromes.[13,30] As our understanding of genotype-phenotype relationships improves, genetic screening of these patients may become increasingly useful for prognostication, genetic counseling and treatment decision making.[13] Our study demonstrates varying incidences and severities of tracheal cartilage malformations among four genotypes associated with *Fgfr2* craniosynostosis syndromes and TCS phenotypes. This strengthens the notion that genotype information in craniosynostosis may help guide airway evaluation and intervention decisions.

Several limitations are worth noting. There were substantially fewer $Fgfr2^{+/Y394C}$, $Fgfr2^{+/S252W}$ and $Fgfr2^{+/P253R}$ specimens than $Fgfr2^{C342Y/+}$. It is possible that more severely affected tracheas would have been present in other groups, had greater numbers of specimens been available. The mouse model of Beare-Stevenson syndrome ($Fgfr2^{+/Y394C}$) was characterized by Wang et al., and while several abnormalities were noted, tracheal morphology was not described.[14] Though TCS has been seen in the human $FGFR2^{Y375C}$ variant, our results suggest that they are not present or are present at low frequency in the mouse model.[3,31] Among Apert syndrome-associated FGFR2 mutations, Wang et al. observed TCS in 8% of $Fgfr2^{+/S252W}$ mice.[16] The malformation has not been described in $Fgfr2^{+/P253R}$ mice.[17] Additional variability may have been introduced by using mice with different genetic backgrounds. We attempted to control for this by using line-specific control groups, but variability could not be controlled in comparisons between the *Fgfr2* variants

with differing genetic backgrounds (i.e. *Fgfr2*^{C342Y} – CD1 vs other *Fgfr2* variant groups – C57Bl/6J). While at least 10 other FGFR2 mutations have been associated with TCS in humans,[3] our study utilized models of four classic TCS-associated mutations available to us at the time of this study. A homozygous model was only available for the *Fgfr2*^{C342Y} variant.

Conclusion:

TCS is a common life-threatening airway malformation found in patients with syndromic craniosynostosis. This study highlights the variability of TCS formation seen in murine models of *Fgfr2*-associated craniosynostosis syndromes. The *Fgfr2*^{C342Y} variant appears to be associated with tracheal cartilage abnormalities occurring more frequently and with greater severity than other tested variants. The presence of higher risk genotypes for tracheal cartilage malformations supports further study of these lines and the investigation of other *Fgfr2* variants to better understand their role in tracheal development and TCS formation. This study lays a foundation for future researchers in understanding the relationships between specific FGFR2 mutations and TCS phenotypes.

Supplementary Material

Refer to Web version on PubMed Central for supplementary material.

Acknowledgments:
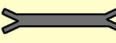
References:

1. Alli A, Gupta S, Elloy MD, Wyatt M. Laryngotracheal anomalies in children with syndromic craniosynostosis undergoing tracheostomy. J Craniofac Surg. 2013;24(4):1423–1427. doi:10.1097/SCS.0b013e3182953b43 [PubMed: 23851823]

2. Inglis AF, Kokesh J, Siebert J, Richardson MA. Vertically Fused Tracheal Cartilage: An Underrecognized Anomaly. Arch Otolaryngol Head Neck Surg. 1992;118(4):436–438. doi:10.1001/archotol.1992.01880040102017 [PubMed: 1554475]

3. Wenger TL, Dahl J, Bhoj EJ, et al. Tracheal cartilaginous sleeves in children with syndromic craniosynostosis. Genet Med. 2017;19(1):62–68. doi:10.1038/gim.2016.60 [PubMed: 27228464]

4. Lertsburapa K, Schroeder JW, Sullivan C. Tracheal cartilaginous sleeve in patients with craniosynostosis syndromes: A meta-analysis. J Pediatr Surg. 2010;45(7):1438–1444. doi:10.1016/j.jpedsurg.2009.09.005 [PubMed: 20638521]

5. Stater BJ, Oomen KPQ, Modi VK. Tracheal cartilaginous sleeve association with syndromic midface hypoplasia. JAMA Otolaryngol - Head Neck Surg. 2015;141(1):73–77. doi:10.1001/jamaoto.2014.2790 [PubMed: 25375853]

6. Eswarakumar VP, Lax I, Schlessinger J. Cellular signaling by fibroblast growth factor receptors. Cytokine Growth Factor Rev. 2005;16(2 SPEC. ISS.):139–149. doi:10.1016/j.cytogfr.2005.01.001 [PubMed: 15863030]

7. Robin NH, Falk MJ, Haldeman-Englert CR. FGFR-Related Craniosynostosis Syndromes. 1998 Oct 20 [Updated 2011 Jun 7]. In: Adam MP, Ardinger HH, Pagon RA, et al., editors. GeneReviews® [Internet]. Seattle WA): University of Washington, Seattle; 1993–2019.; 1993.

8. Snyder-Warwick AK, Perlyn CA, Pan J, Yu K, Zhang L, Ornitz DM. Analysis of a gain-of-function FGFR2 Crouzon mutation provides evidence of loss of function activity in the etiology of cleft palate. Proc Natl Acad Sci U S A. 2010;107(6):2515–2520. doi:10.1073/pnas.0913985107 [PubMed: 20133659]

9. Wilkie AOM. Craniosynostosis: Genes and mechanisms. Hum Mol Genet. 1997;6(10 REV. ISS.):1647–1656. doi:10.1093/hmg/6.10.1647 [PubMed: 9300656]

10. Webster MK, Donoghue DJ. FGFR activation in skeletal disorders: Too much of a good thing. Trends Genet. 1997;13(5):178–182. doi:10.1016/S0168-9525(97)01131-1 [PubMed: 9154000]

11. Przylepa KA, Paznekas W, Zhang M, et al. Fibroblast growth factor receptor 2 mutations in Beare–Stevenson cutis gyrata syndrome. Nat Genet. 1996;13(4):492–494. doi:10.1038/ng0896-492 [PubMed: 8696350]

12. Ibrahimi OA, Zhang F, Eliseenkova AV, Itoh N, Linhardt RJ, Mohammadi M. Biochemical analysis of pathogenic ligand-dependent FGFR2 mutations suggests distinct pathophysiological mechanisms for craniofacial and limb abnormalities. Hum Mol Genet. 2004;13(19):2313–2324. doi:10.1093/hmg/ddh235 [PubMed: 15282208]

13. Cunningham ML, Seto ML, Ratisoontorn C, Heike CL, Hing AV. Syndromic craniosynostosis: From history to hydrogen bonds. Orthod Craniofac Res. 2007;10(2):67–81. doi:10.1111/j.1601-6343.2007.00389.x [PubMed: 17552943]

14. Wang Y, Zhou X, Oberoi K, et al. p38 inhibition ameliorates skin and skull abnormalities in Fgfr2 Beare-Stevenson mice. J Clin Invest. 2012;122(6):2153–2164. doi:10.1172/JCI62644 [PubMed: 22585574]

15. Eswarakumar VP, Horowitz MC, Locklin R, Morriss-Kay GM, Lonai P. A gain-of-function mutation of Fgfr2c demonstrates the roles of this receptor variant in osteogenesis. Proc Natl Acad Sci U S A. 2004;101(34):12555–12560. doi:10.1073/pnas.0405031101 [PubMed: 15316116]

16. Wang Y, Xiao R, Yang F, et al. Abnormalities in cartilage and bone development in the Apert syndrome FGFR2+/S252W mouse. Development. 2005;132(15):3537–3548. doi:10.1242/dev.01914 [PubMed: 15975938]

17. Wang Y, Sun M, Uhlhorn VL, et al. Activation of p38 MAPK pathway in the skull abnormalities of Apert syndrome Fgfr2+P253R mice. BMC Dev Biol. 2010;10:22. doi:10.1186/1471-213X-10-22 [PubMed: 20175913]

18. Rigueur D, Lyons KM. Whole-Mount Skeletal Staining. In: Hilton MJ, ed. Skeletal Development and Repair: Methods and Protocols. Vol 1130. Methods in Molecular Biology Humana Press; 2014:113–121. doi:10.1007/978-1-62703-989-5_9

19. Premakumar Y, Griffin MF, Szarko M. Morphometric characterisation of human tracheas: Focus on cartilaginous ring variation. BMC Res Notes. 2018;11(1). doi:10.1186/s13104-018-3123-1

20. Rasband WS. ImageJ, Version 1.52a. U. S. National Institutes of Health https://imagej.nih.gov/ij/, 1997–2018

21. Lesciotto KM, Perrine SMM, Kawasaki M, et al. Phosphotungstic acid enhanced microCT: optimized protocols for embryonic and early postnatal mice. Dev Dyn Off Publ Am Assoc Anat. 2020;249(4):573–585. doi:10.1002/dvdy.136

22. Fedorov A, Beichel R, Kalpathy-Cramer J, et al. 3D Slicer as an image computing platform for the Quantitative Imaging Network. Magn Reson Imaging. 2012;30(9):1323–1341. doi:10.1016/j.mri.2012.05.001 [PubMed: 22770690]

23. Zaiontz C Real Statistics Resource Pack software. Published online 2015.

24. Hockstein NG, McDonald-McGinn D, Zackai E, Bartlett S, Huff DS, Jacobs IN. Tracheal anomalies in Pfeiffer syndrome. Arch Otolaryngol - Head Neck Surg. 2004;130(11):1298–1302. doi:10.1001/archotol.130.11.1298 [PubMed: 15545585]

25. Chen JC, Holinger LD. Congenital tracheal anomalies: Pathology study using serial macrosections and review of the literature. Fetal Pediatr Pathol. 1994;14(3):513–537. doi:10.3109/15513819409024281

26. Noorily MR, Farmer DL, Belenky WM, Philippart AI. Congenital tracheal anomalies in the craniosynostosis syndromes. J Pediatr Surg. 1999;34(6):1036–1039. doi:10.1016/S0022-3468(99)90787-X [PubMed: 10392932]

27. Zenner K, Bonilla-Velez J, Johnson K, Bly RA. Slide tracheoplasty to repair stenotic tracheal cartilaginous sleeve with advanced surgical planning. Otolaryngol Neck Surg. Published online April 14, 2020:0194599820915469. doi:10.1177/0194599820915469

28. Holmes G, O'Rourke C, Motch Perrine SM, et al. Midface and upper airway dysgenesis in FGFR2-related craniosynostosis involves multiple tissue-specific and cell cycle effects. Dev Camb Engl. 2018;145(19). doi:10.1242/dev.166488

29. Motch Perrine SM, Wu M, Stephens NB, et al. Mandibular dysmorphology due to abnormal embryonic osteogenesis in FGFR2-related craniosynostosis mice. Dis Model Mech. 2019;12(5). doi:10.1242/dmm.038513

30. Mullikcn JB, Steinberger D, Kunze S, Müller U. Molecular diagnosis of bilateral coronal synostosis. Plast Reconstr Surg. 1999;104(6):1603–1615. doi:10.1097/00006534-199911000-00001 [PubMed: 10541159]

31. Seki E, Enomoto K, Tanoue K, Tanaka M, Kurosawa K. Tracheal cartilaginous sleeve in patients with Beare-Stevenson syndrome. Congenit Anom. 2020;60(3):97–99. doi:10.1111/cga.12352

Assigned Code	Tracheal ring shape	Description	Frequency (%)
A		"Classic ring" – Singular straight band of tracheal cartilage.	100%
B		"Bifurcated ring" – Singular straight band of cartilage that crosses midline and bifurcates into two distinct bands.	61%
C		"Connected rings" – Two distinct rings of cartilage connected by a narrow band of cartilage.	12%
D		"Fused rings" – Two distinct rings of cartilage with wide common connection.	3%
E		"Thickened ring" – One distinct cartilaginous ring with thickened medial segment.	9%
F		"Slitted ring" – Thickened ring of cartilage with slit in middle.	18%
G		"Pentagonal ring" = Distinct ring of cartilage with perpendicularly directed point near the middle.	55%
H		"Ring piece" – Small piece of tracheal cartilage that is distinct from, though may be closely approximated to, a larger ring of cartilage.	24%
I		"Incomplete ring" – Distinct straight band of cartilage that does not span the entire width of the trachea.	49%
J		"Segmented ring" – Straight band of cartilage that has missing segment near the middle.	0%
K		"Merged rings" – Two distinct and complete bands of cartilage that cross midline and merge into a single band on the contralateral side.	49%
L		"Incomplete merged rings" – One distinct incomplete ring that merges with either another incomplete ring or a complete ring.	15%
M		"Laterally connected rings" – Two distinct rings of cartilage that are connected by a thin band at their most lateral aspect.	12%
N		"Double bifurcated ring" – Singular cartilaginous ring of normal thickness that spans the majority of the tracheal width before bifurcating on both ends.	9%
O		"Merged Bifurcated Ring" - Merged ring that bifurcates at the contralateral end.	6%
P		"Complete cartilaginous sleeve" – Uninterrupted sleeve of cartilage spanning the entire width of the trachea, for an entire tracheal segment.	0%
Q		"Partially sleeved rings" – All rings fused with only small areas of non-cartilaginous structures, spanning an entire tracheal segment.	0%
Z	Other	Ring shape that either does not conform to or is a combination of the above listed descriptions.	36%

Figure 1:

Tracheal ring types, their assigned codes, descriptions and frequencies at which they were observed in control specimens. "Normal" tracheal ring types (frequency in controls ≥ 20%) are highlighted in green whereas "Abnormal" and "Sleeve-Type" are highlighted in yellow and red, respectively.

Note: Sleeve-type segments are classified both as "Abnormal" and "Sleeve-Type" for analyses.
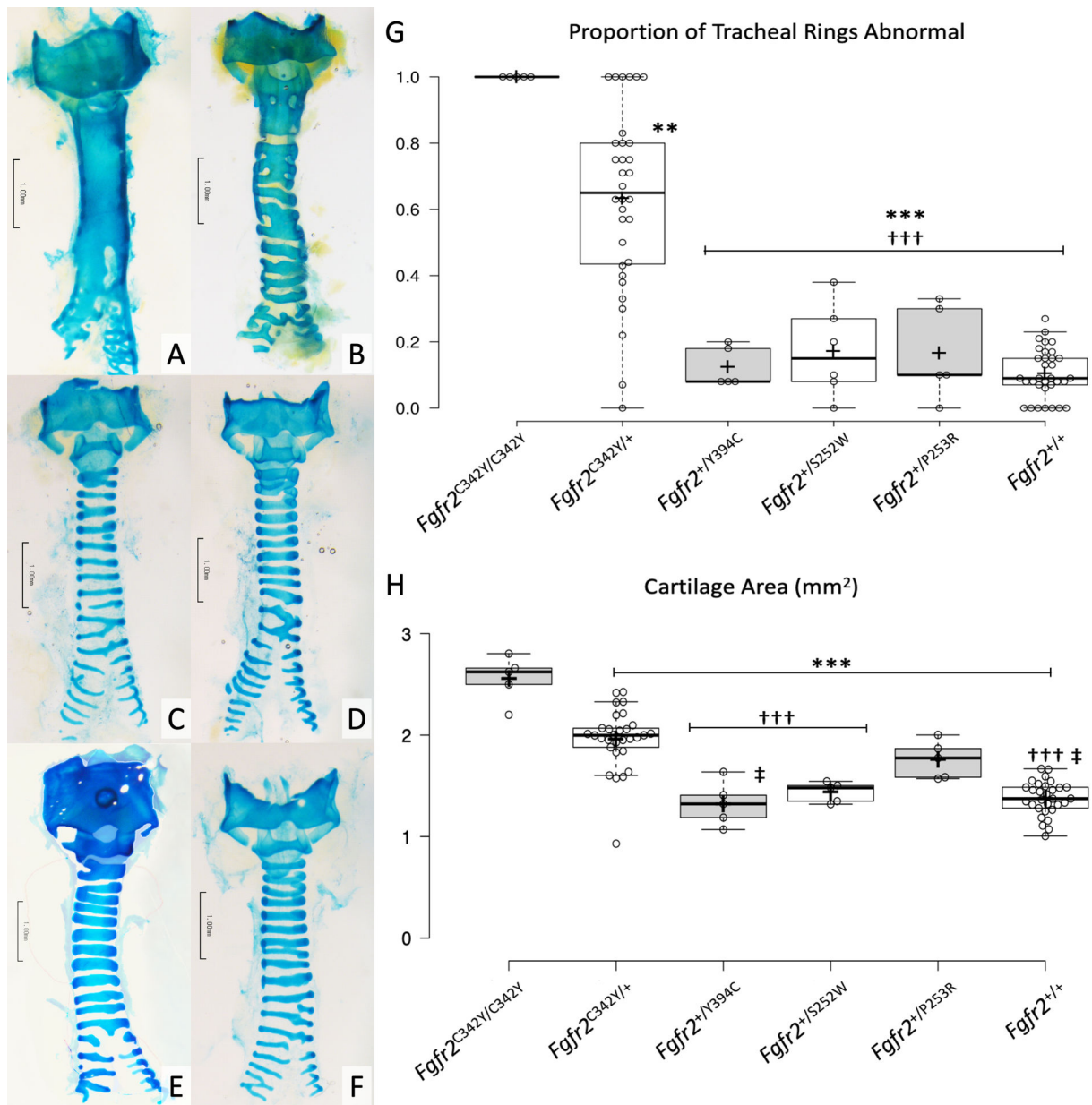
Figure 2:

Panels A-F represent alcian blue stained whole-mount specimens, A) $Fgfr2^{C342Y/C342Y}$, B) $Fgfr2^{C342Y/+}$, C) $Fgfr2^{+/Y394C}$, D) $Fgfr2^{+/S252W}$, E) $Fgfr2^{+/P253R}$ and F) $Fgfr2^{+/+}$. Scale bars = 1.0 mm.

Panels G and H demonstrate box plots representing the proportion of tracheal rings that were abnormal and cartilage area, respectively. Center lines show the medians; box limits indicate the 25th and 75th percentiles; whiskers extend 1.5 times the interquartile range from the 25th and 75th percentiles; plus signs represent sample means; data points are plotted as open circles.
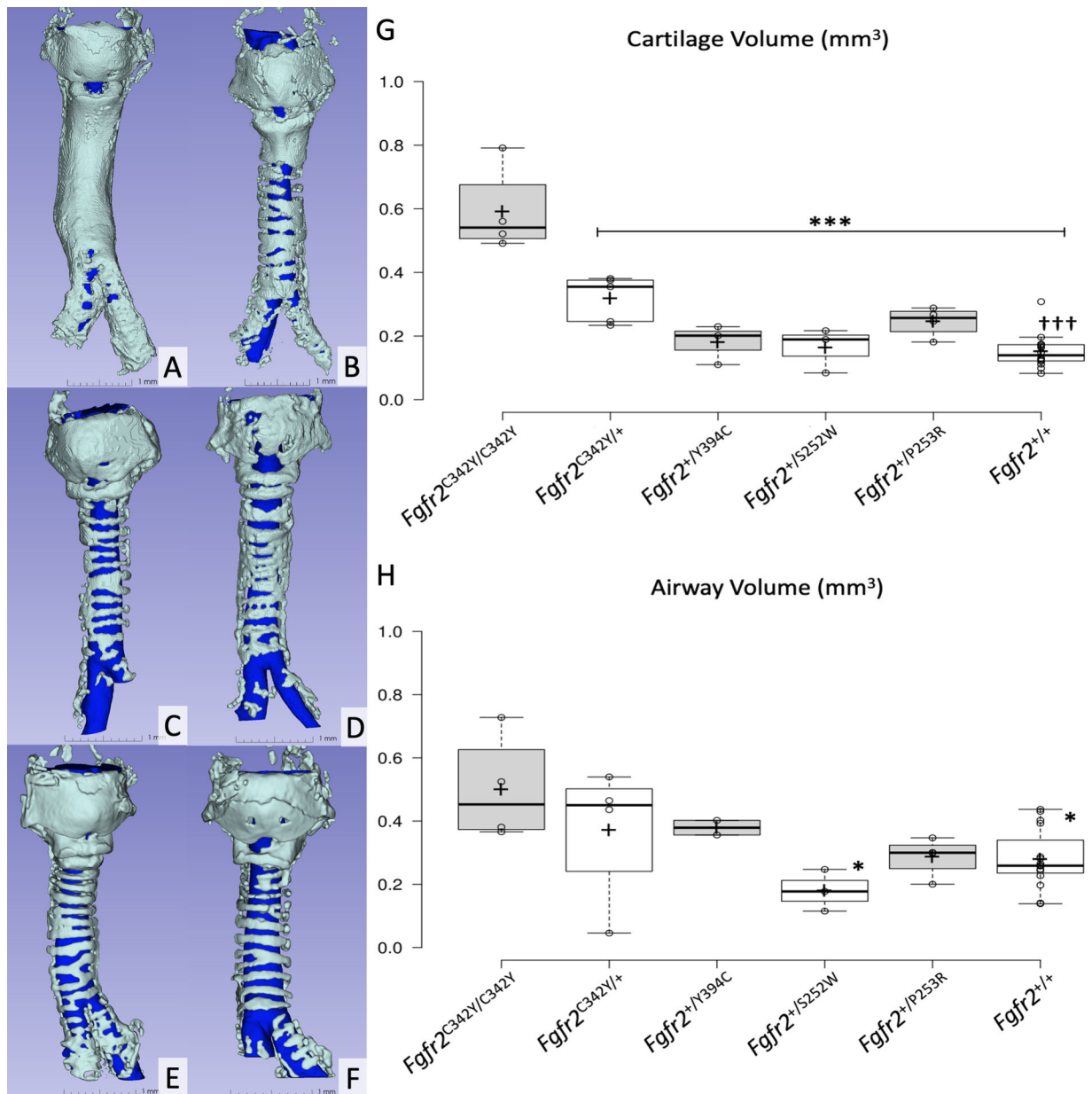
** $p < .01$ vs $Fgfr2^{C342Y/C342Y}$

*** $p < .001$ vs $Fgfr2^{C342Y/C342Y}$

††† $p < .001$ vs $Fgfr2^{C342Y/+}$

‡ $p < .05$ vs $Fgfr2^{+/P253R}$

Figure 3:

Panels A-F represent 3D-reconstructions of microcomputed-tomography specimens, A) $Fgfr2^{C342Y/C342Y}$, B) $Fgfr2^{C342Y/+}$, C) $Fgfr2^{+/Y394C}$, D) $Fgfr2^{+/S252W}$, E) $Fgfr2^{+/P253R}$ and F) $Fgfr2^{+/+}$. Scale bars = 1.0 mm.

Panels G and H demonstrate box and whisker plots representing cartilage volume and airway volume, respectively. Center lines show the medians; box limits indicate the 25th and 75th percentiles; whiskers extend 1.5 times the interquartile range from the 25th and 75th percentiles; crosses represent sample means; data points are plotted as open circles.

* $p < .05$ vs $Fgfr2^{C342Y/C342Y}$

*** $p < .001$ vs $Fgfr2^{C342Y/C342Y}$

††† $p < .001$ vs $Fgfr2^{C342Y/+}$
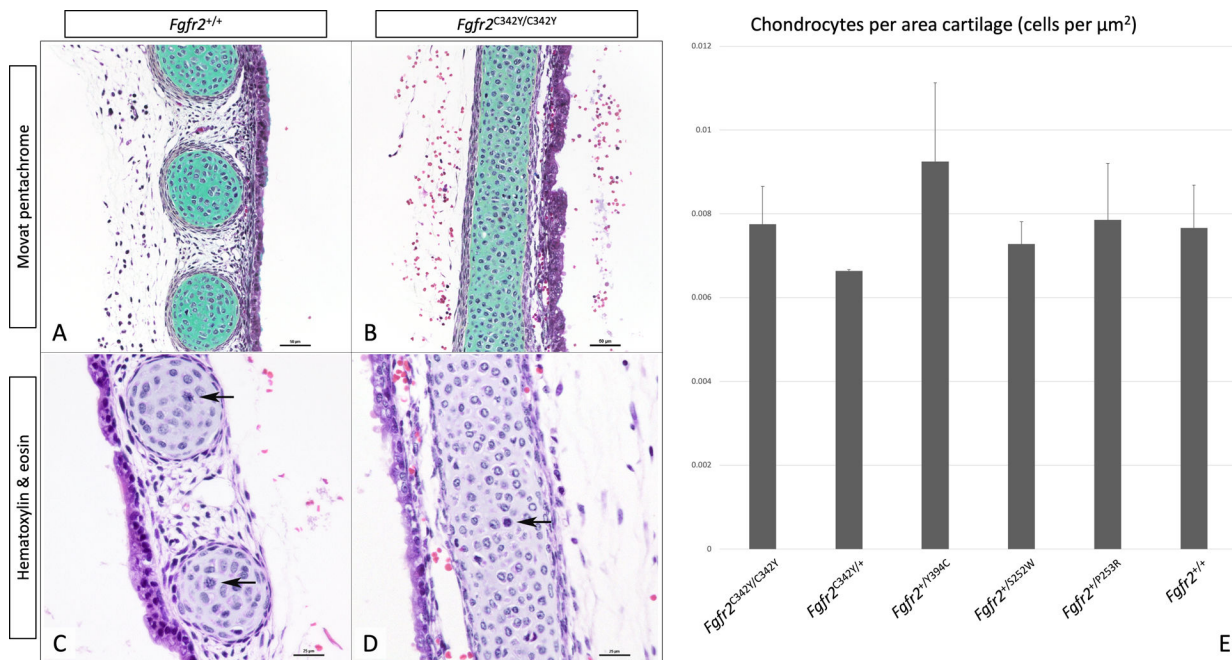
Figure 4:
Representative images of Movat pentachrome stain (panels A, B) and hematoxylin & eosin stain (panels C, D) of *Fgfr2*^{+/+} (panels A, C), and *Fgfr2*^{C342Y/C342Y} (panels B, D) highlight cartilage (stained green) and mitotic figures (arrows). Panel E shows a bar graph representing the number of chondrocytes per area of hyaline cartilage as assessed on 5 random images taken at 40x for 2 samples per group. Error bars represent standard deviations. Scale bars = 50 μm for panels A, B, and 25 μm for panels C, D.

Table 1:

Proportion of abnormal rings per trachea on tracheal morphology evaluation data comparisons between *Fgfr2* gene variants and controls (pooled). *n* – number of samples per group. SD – standard deviation.

Group	*n*	mean (± SD)	p-value
		Abnormal Rings per Trachea (mean proportion)	*<.001*
*Fgfr2*C342Y/C342Y	5	100% (±0%)	
*Fgfr2*C342Y/+	32	63% (±27%)	
Fgfr2+/Y394C	5	12% (±6%)	
Fgfr2+/S252W	6	17% (±14%)	
Fgfr2+/P253R	5	17% (±14%)	
Fgfr2+/+	33	10% (±8%)	

Table 2:

Whole-mount cartilage area data comparisons between *Fgfr2* gene variants and controls (pooled). *n* – number of samples per group. SD – standard deviation.

Group	*n*	mean (± SD)	p-value
		Cartilage Area (mm^2)	*<.001*
Fgfr2$^{C342Y/C342Y}$	5	2.56 (±0.23)	
Fgfr2$^{C342Y/+}$	30	1.96 (±0.29)	
Fgfr2$^{+/Y394C}$	5	1.32 (±0.22)	
Fgfr2$^{+/S252W}$	5	1.44 (±0.10)	
Fgfr2$^{+/P253R}$	5	1.76 (±0.18)	
Fgfr2$^{+/+}$	30	1.38 (±0.17)	

Table 3:

Microcomputed-tomography data comparisons between *Fgfr2* gene variants and controls (pooled). *n* – number of samples per group. SD – standard deviation.

Group	*n*	mean (± SD)	p-value
		Cartilage Volume (mm^3)	*<.001*
Fgfr2$^{C342Y/C342Y}$	4	0.59 (±0.14)	
Fgfr2$^{C342Y/+}$	5	0.32 (±0.07)	
Fgfr2$^{+/Y394C}$	3	0.18 (±0.06)	
Fgfr2$^{+/S252W}$	3	0.16 (±0.07)	
Fgfr2$^{+/P253R}$	4	0.25 (±0.05)	
Fgfr2$^{+/+}$	16	0.15 (±0.05)	
		Airway Volume (mm^3)	*.02*
Fgfr2$^{C342Y/C342Y}$	4	0.50 (±0.17)	
Fgfr2$^{C342Y/+}$	4	0.37 (±0.22)	
Fgfr2$^{+/Y394C}$	2	0.38 (±0.03)	
Fgfr2$^{+/S252W}$	3	0.18 (±0.07)	
Fgfr2$^{+/P253R}$	4	0.29 (±0.06)	
Fgfr2$^{+/+}$	16	0.28 (±0.09)	